

## DIFFERENT TYPES OF X-RAY BURSTS FROM GRS 1915+105 AND THEIR ORIGIN

J. S. YADAV<sup>1</sup>, A. R. RAO, P. C. AGRAWAL, B. PAUL

Tata Institute of Fundamental Research, Homi Bhabha Road, Mumbai 400 005, India

AND

S. SEETHA, AND K. KASTURIRANGAN

ISRO Satellite Centre, Airport Road, Vimanpura P.O. Bangalore 560 017, India

*To appear in June 1, 1999 issue of The Astrophysical Journal*

### ABSTRACT

We report the X-ray observations of the Galactic X-ray transient source GRS 1915+105 with the Pointed Proportional Counters of the Indian X-ray Astronomy Experiment (IXAE) onboard the Indian satellite IRS-P3, which show remarkable richness in temporal variability. The observations were carried out on 1997 June 12 - 29 and August 7 - 10, in the energy range of 2–18 keV and revealed the presence of very intense X-ray bursts. All the observed bursts have a slow exponential rise, a sharp linear decay, and they can broadly be put in two classes: irregular and quasi-regular bursts in one class, and regular bursts in another class. The regular bursts are found to have two distinct time scales and they persist over extended durations. There is a strong correlation between the preceding quiescent time and the burst duration for the quasi-regular and irregular bursts. No such correlation is found for the regular bursts. The ratio of average flux during the burst time to the average flux during the quiescent phase is high and variable for the quasi-regular and irregular bursts while it is low and constant for the regular bursts. We present a comprehensive picture of the various types of bursts observed in GRS 1915+105 in the light of the recent theories of advective accretion disks. We suggest that the peculiar bursts that we have seen are characteristic of the change of state of the source. The source can switch back and forth between the low-hard state and the high-soft state near critical accretion rates in a very short time scale, giving rise to the irregular and quasi-regular bursts. The fast time scale for the transition of the state is explained by invoking the appearance and disappearance of the advective disk in its viscous time scale. The periodicity of the regular bursts is explained by matching the viscous time scale with the cooling time scale of the post shock region. A test of the model is presented using the publicly available 13–60 keV RXTE/PCA data for irregular and regular bursts concurrent with our observations. It is found that the 13–60 keV flux relative to the 2–13 keV flux shows clear evidence for state change between the quiescent phase and the burst phase. The value of this ratio during burst is consistent with the values observed during the high-soft state seen on 1997 August 19 while its value during quiescent phase is consistent with the values observed during the low-hard state seen on 1997 May 8.

*Subject headings:* accretion, accretion disks — binaries: close — black hole physics — X-rays: bursts, stars — stars: individual GRS 1915+105

<sup>1</sup>Send offprint request to: jsyadav@tifr.res.in

## 1. INTRODUCTION

The X-ray transient source GRS 1915+105 was discovered in 1992 with the WATCH all sky X-ray monitor onboard the GRANAT satellite (Castro-Tirado et al. 1994). Superluminal motions of two symmetric radio emitting jets of GRS 1915+105 were discovered by Mirabel & Rodriguez (Mirabel & Rodriguez 1994). Several features in the observed properties of GRS 1915+105 such as the Power Density Spectra (PDS) with the QPO feature, a hard X-ray tail and the subsecond time variability, are typical characteristics of black hole binaries. The X-ray intensity is found to be more than  $10^{39}$  erg s $^{-1}$  (based on an assumed distance of 12.5 kpc) for extended periods which is super-Eddington luminosity for a neutron star (Mirabel & Rodriguez 1994). The other Galactic source of superluminal jets, GRO J1655-40, has been shown to harbor a compact object of mass  $\sim 7 M_{\odot}$  (Orosz & Bailyn 1997). The combination of relativistic jets and a central black hole has earned these two objects the name “microquasars” as they seem to be stellar mass analogs of the massive black hole systems in quasars and other active galactic nuclei (AGNs). These microquasars have opened the possibility of studying phenomena in our Galaxy that until recently were believed to be restricted to distant quasars and a few AGNs. In particular, it has been realized that since the characteristic dynamic times in the flow of matter onto a black hole are proportional to its mass, the events with intervals of minutes in a microquasar could correspond to analogous phenomena with duration of thousands of years in a quasar of  $10^9 M_{\odot}$ .

GRS 1915+105 was observed to be X-ray active in 1994 using BATSE instrument. The source went into a very high X-ray intensity state in early 1996 and was observed on several occasions by the Pointed Proportional Counters (PPCs) of the Indian X-ray Astronomy Experiment (IXAE) (Agrawal et al. 1997; Paul et al. 1997), the Proportional Counter Array (PCA) and the All Sky Monitor (ASM) of the Rossi X-ray Timing Explorer (RXTE) (Bradt 1996). The X-ray intensity was found to vary on a variety of time scales and the light curve showed a complicated pattern of dips and rapid transitions between high and low intensity (Greiner et al. 1996; Belloni et al. 1997b; Taam et al. 1997). PPC observations of GRS 1915+105 in its low hard state in 1996 July showed intensity variations by a fac-

tor of 2 to 3 at 100–400 ms time scale (Paul et al. 1997; Paul et al. 1998a). Strong (rms variability 9%) and narrow ( $\frac{\nu}{\delta\nu} \approx 5$ ) Quasi-Periodic Oscillations (QPOs) of varying frequency were discovered in GRS 1915+105 with the PPC observations (Agrawal et al. 1996). Quasi-regular X-ray and infrared (IR) flares with a spacing of  $\sim 30$  minutes, were observed during simultaneous X-ray/IR observations (Eikenberry et al. 1998). These observations suggest that IR flares are signatures of plasma ejection in the inner part of the accretion disk which are termed as “baby jets” analog to the much larger superluminal ejection events. At later times, the X-ray flares decouple from IR flares ruling out thermal reprocessing of the X-rays as the source of the IR flares. Another simultaneous observations of GRS 1915+105 in the X-ray, IR, and radio wavelengths confirm that the IR and radio flares are associated with the X-ray dips (Mirabel et al. 1998).

The most compelling evidence for the existence of a black hole in Galactic X-ray binaries normally comes from the measured mass function which indicates that the mass of the compact object is much larger than that permitted for a neutron star. In the absence of measured binary parameters (like in the case of GRS 1915+105) phenomenological arguments are normally used, which, though compelling for a class of objects, are not conclusive enough for individual cases. This is mainly due to the fact that the accretion disk around a black hole has properties quite similar to that around a low magnetic field neutron star (Tanaka and Lewin 1995). Recent progress in the understanding of accretion onto black holes has suggested that the black hole accretion disks are cooled by advection in their innermost parts (Chakrabarti 1996a; Abramowicz and Percival 1997; Narayan et al. 1998). Based on the new accretion theories involving advection, features in black hole accretion which uniquely distinguishes them from low magnetic field accreting neutron star, have been identified. Narayan et al. (1997a) have argued that advective cooling can occur throughout the disk for black hole accretion providing a unique way of identifying black hole binaries in their quiescent state. Chakrabarti and Titarchuk (1995) have argued that in the very high state of the sources, black hole binaries should have a unique extended power law due to bulk comptonisation (see also Laurent and Titarchuk 1998). In an earlier paper (Paul et al.

TABLE 1  
THE GRS 1915+105 OBSERVATIONS BY IXAE DURING 1997 JUNE-AUGUST.

DOY	Date	Start time	End time	Orbits	time(s)	Mode	PPC
164	Jun 12	17:36:57	19:27:24	2	1600	M	1 2 3
168	Jun 16	14:21:46	18:04:10	4	1880	M	1 2 3
169	Jun 17	13:59:54	17:42:50	3	2760	M	- 2 3
169	Jun 18	11:55:40	15:40:19	3	1630	M	- 2 3
170	Jun 19	11:35:54	15:20:26	3	1530	M	1 2 3
173	Jun 21	10:59:28	17:55:38	5	5070	N	1 2 3
174	Jun 22	12:12:24	19:20:50	5	5300	N	1 2 3
175	Jun 23	11:52:08	18:59:46	5	5400	N	1 2 3
176	Jun 24	11:30:15	18:38:52	5	5700	N	1 2 3
177	Jun 25	11:12:05	18:18:02	5	5700	N	1 2 3
178	Jun 26	10:50:03	17:56:00	5	5220	N	1 2 3
179	Jun 27	15:30:57	17:34:22	3	2770	M	- 2 3
181	Jun 29	11:27:23	15:11:55	3	2490	M	- - 3
220	Aug 07	11:25:19	18:37:51	5	5750	N	1 2 3
221	Aug 08	10:05:49	17:17:19	5	4740	N	1 2 3
222	Aug 09	10:49:03	17:52:31	5	4850	N	1 2 3
223	Aug 10	12:13:19	19:16:15	5	5360	N	1 2 3

DOY = day of year, M = medium mode, N = Nominal mode

1998b, hereafter Paper I), we presented a possible evidence for the direct detection of advection in GRS 1915+105. This is based on the detection of regular and persistent X-ray bursts which have a slow exponential rise, sharp decay and hardening of the spectrum as the burst progresses.

In this paper, we present a detailed analysis of all the IXAE observations of GRS 1915+105 during 1997 June-August. We specially study temporal variations on a time scale from few seconds to few minutes. In the following sections, we describe the observations and the properties of 1889 bursts observed with PPCs. We discuss our results in the framework of advective accretion disk models.

## 2. OBSERVATIONS

The Indian X-ray Astronomy Experiment (IXAE) onboard the Indian satellite IRS-P3 consists of three identical pointed proportional counters (PPCs) and one X-ray sky monitor and it was launched on 1996 March 21 from Shriharikota Range, India. The observations were carried out using all the 3 PPCs of IXAE. The PPCs are filled with argon-methane mixture at 800 torr pressure and have a total area of 1200 cm<sup>2</sup>. The operating energy range is between 2 keV and 18 keV and

a passive collimator restricts the field of view to  $2.3^\circ \times 2.3^\circ$ . The energy resolution is  $\approx 22(\frac{E}{6})^{-\frac{1}{2}}\%$  at E keV with a detection efficiency of about 65% at 6 keV and 10% at 15 keV. Each PPC is a multilayer unit consisting of 54 anode cells of size 1.1 cm  $\times$  1.1 cm arranged in 3 identical layers. The end cells of each layer and all the 18 anodes of the third layer are connected together and operated as a veto layer for the top two layers which constitute the X-ray detection volume. The alternate anodes in each of the two X-ray detection layers are joined together and operated in mutual anti-coincidence to reject charged particle induced background. Each PPC has its own front-end electronics and a processing electronics. The processing electronics selects the genuine events based on the pre-determined logic conditions. An 8086 microprocessor based system handles the data from each PPC and stores them in 4 Mbits of memory. The data storage is done in different modes which can be set by commands. For further details of the PPCs and the observation methodology see Rao et al. (1998).

The IRS-P3 satellite is in a circular orbit at an altitude of 830 km and inclination of 98°. A star tracker onboard the IRS-P3 satellite co-aligned

with the viewing axes of the proportional counters is used for pointing towards the X-ray sources with a pointing accuracy of about  $0.1^\circ$ . The high inclination and high altitude orbit is found to be very background prone and the useful observation time is limited to the latitude ranges typically from  $-30^\circ$  S to  $+50^\circ$  N. Further, the South Atlantic Anomaly (SAA) region restricts the observation to about 5 of the 14 orbits per day. Observations with the PPCs are usually made in about 5 orbits of the satellite every day in the nominal mode (N) with 1.0 s time resolution and each observation has a duration of about 20 minutes. In the medium mode (M) with time resolution of 0.1 s, data are usually available only for three orbits due to the limited size of the onboard data storage unit. During 17 days of observations from June 12 to August 10, data from 71 orbits were collected and a total of 67,750 seconds of useful exposure time was obtained. A summary of the observations is given in Table 1.

### 3. THE BURST PROFILES

Intense X-ray bursts are observed through out the PPC observations over the period of 1997 June 12-29 and August 7-10. These bursts can broadly be put into two classes: regular bursts lasting typically for a few days and centered around a fixed period with low dispersion ( $\delta P/P \sim 5 - 10\%$ ) and irregular bursts with no fixed periodicity ( $\delta P/P \geq 50\%$ ). The period of regular bursts shows two distinct time scales during our observations and quasi-regular bursts with properties in between those observed for the regular and irregular bursts have also been seen. The observed bursts are, therefore, classified into four types: (a) regular bursts having a slow rise and fast decay lasting for  $\sim 15$  s and recurring every 21 s, (b) regular bursts, having a slow rise and sharp decay lasting for  $\sim 20$  s and recurring every 46 s, (c) quasi-regular bursts of variable duration, slow rise and sharp decay, and (d) irregular bursts, with duration of a few tens to a few hundred seconds, followed by sharp decay. Sharp decay is a common feature of all the bursts. All the regular bursts usually have two peak structure while quasi-regular and irregular bursts show multi-peak structure.

Representative 2–18 keV light curves, added for all the PPCs except on June 27 when only PPC 2 & 3 were on, of 300 s duration obtained on different days are shown in top four panels of Figure 1.

These burst profiles were detected independently in each of the PPCs. All the panels in the figure have similar Y-axis scales. Regular bursts of  $\sim 21$  s recurrence time were detected during August 7-10 with second peak being prominent and a sharp narrow dip between the two peaks; regular bursts of  $\sim 46$  s recurrence time were detected during June 12–17 and again during June 22–26 with first peak being prominent; quasi-irregular bursts were seen during June 19–21 and irregular bursts were detected on June 18 and June 27-29. In the second panel (from bottom), we show regular bursts observed on 1997 June 22. The time zero corresponds to 1997 June 22, 19:10 UT with the PPCs. Similar burst profiles are seen from publicly available 2–13 keV RXTE/PCA data of 1997 June 22 which are shown in the bottom panel of Figure 1. The time zero corresponds to 1997 June 22, 19:35 UT. Remarkable similarity between temporal profiles of regular bursts observed by PPCs and independently by the PCA about 25 minutes later is apparent from the first and second panels (from the bottom) of Figure 1. A secondary peak near the end of the bursts is a common feature of all the bursts. The quasi-regular and irregular long bursts show higher variability near the end of the burst and the burst duration is correlated to the quiescent state period just prior to the burst which we shall discuss in detail in the next section.

All the bursts start with a well defined sharp peak and decay faster than they rise. We define a burst event as a full cycle of one quiescent interval followed by one burst. The recurrence time is the sum of quiescent time and the burst duration. With this definition there is no interval between burst events. This defines the individual burst events adequately for the regular and quasi-regular bursts. In the case of irregular bursts, we put additional criterion that separate events are considered to be only those whose quiescent count rate goes below  $250 \text{ counts s}^{-1}$  for individual PPC in the total 2.0-18.0 keV energy band. We measured the start of a burst event (corresponding to the end of the previous one) as the time of the small dip at the end of the decay. Since all the bursts start with a sharp peak, the time of the peak can be taken as the separation between the quiescent phase and the burst phase. We have marked the positions in the third panel of Figure 1 for a burst event: beginning of quiescent phase (preceding) is marked by 'a', end of the quies-

TABLE 2  
SUMMARY OF CHARACTERISTICS OF DIFFERENT TYPE OF BURSTS FROM GRS 1915+105.

Type of burst	Mean recurrence time or interval (s)	No of bursts	Norm. <sup>a</sup> q. flux	Mean q. H R <sup>b</sup>	Mean b. H R <sup>b</sup>	Date of observation
reg. bursts	21 $\pm$ 3	995	2.87	1.28 $\pm$ 0.05	2.2 $\pm$ 0.2	Aug 7-10
reg. bursts	46 $\pm$ 5	738	1.75	0.98 $\pm$ 0.02	1.2 $\pm$ 0.1	Jun 12-17 & Jun 22-26
quasi-reg. bursts	from 50 to 90	115	1.2	0.94 $\pm$ 0.02	1.5 $\pm$ 0.1	Jun 19-21
irreg. bursts	from 18 to 350	67	1.0	0.94 $\pm$ 0.02	1.5 $\pm$ 0.1	Jun 18 & June 27-29

q. = quiescent, b. = burst and H R = hardness ratio

<sup>a</sup>Normalised quiescent flux is normalised to irregular burst

<sup>b</sup>HR is defined as the ratio of counts in 6–18 keV to that in 2–6 keV bands

cent phase and start of burst phase is marked by 'b', and end of the burst phase and start of next quiescent phase (following) is marked by 'c'. We have detected bursts in all our observations. We have calculated mean recurrence time for each day and results are shown in Figure 2. The error bar represents one  $\sigma$  variation in the recurrence time during the observations on each day. The large variations on June 18, June 27, and June 29 represent irregular bursts on these days while small variations on June 12-17, June 22-26 and August 7-10 show regular bursts during these durations. The quasi-regular bursts were observed on June 19 and June 21.

In all the bursts, a dip is present just before the decay of the burst. But the most remarkable feature of our observations is the persistence of the regular bursts for a few days with almost similar shape, structure and period. For both types of regular bursts, the recurrence time for the successive bursts shows a random walk in time instead of any regular pattern. The distribution of burst recurrence time for each day fits well with a Gaussian, with a tail on the higher side, having a width  $\sigma$  of 3-5 s for both the types of regular bursts. In the case of irregular bursts, the distribution of burst recurrence time shows large variations.

To improve the statistical accuracy of the data we have co-added a large number of bursts by matching the last peak. The co-added burst profiles in two different energy ranges (2–6 keV and

6–18 keV) are shown in the top panels while the hardness ratio is shown in the bottom panels of Figure 3 (a & b) for all four types of bursts. We chose to align individual burst of the same type to the last peak in order to keep sharp features during the decay of all the bursts while the sharp features during the rise are smeared out due to the addition of bursts of different duration specially in the case of quasi-regular and irregular bursts. Intensity changes are more prominent at higher energy and the energy spectrum becomes harder as the burst progresses in all types. The burst is hardest near the end of its decay. This is a unique feature of these bursts which distinguishes them from the bursts seen in LMXBs which become softer in the decaying phase (Lewin et al. 1995).

We show the 'rise' and the 'decay' segments of the profile of different type of the bursts in Figure 4. We arbitrarily chose the burst start time at 0 s and the burst end time at 40 s for all types of the bursts to highlight the fact that the slow rise and sharp decay is a common feature of all the bursts. The flux is normalized to the start point for the rise segment and to the end point for the decay segment of the burst profile. The 'rise' and the 'decay' profiles are strikingly similar for both the types of regular bursts observed on August 9 and June 22. A least square fit with a function  $f(t) = a \times \exp^{((t-t_0)/t_r)}$  to the rising segment of the burst profile gives time constant  $t_r = 10$  s

for the regular bursts while it has a value in the range of 5 s to 6 s for the quasi-regular and irregular bursts. The burst decay is consistent with a straight line fit which gives a time constant (defined as the time required to drop from twice the quiescent flux) in the range of 3 s to 7 s.

#### 4. BURST STATISTICS

A summary of the characteristics of different type of bursts is given in Table 2. Also given in the table are mean quiescent and mean burst hardness ratio, defined as the ratio of counts in 6–18 keV to that in 2–6 keV. A total of 995 regular bursts of  $\sim 21$  s recurrence time (in  $\sim 20,700$  s of observation), 738 regular bursts of  $\sim 46$  s recurrence time (in  $\sim 33,560$  s of observation), 115 quasi-irregular bursts (in 6,600 s) and 67 irregular bursts (in  $\sim 6,890$  s) have been detected. The peak intensity varies from 1.5 to 3.5 times the quiescent intensity.

In the case of quasi-regular and irregular bursts, the burst duration is correlated to the quiescent time just prior to the burst. We have measured the quiescent time and the burst duration for all types of bursts according to the definition given in the previous section. Results are shown in Figure 5 along with a least square straight line fit which shows a good correlation between the burst duration and the preceding quiescent time for the quasi-regular and irregular bursts.

We do not see any such correlation for the regular bursts. Inclusion of the regular bursts reduces the correlation coefficient from 0.94 to 0.83 (shown in the inset of Figure 5). Similar plots for the regular bursts of mean recurrence time 21 s and 46 s are shown in the top and the bottom panels of Figure 6 respectively for three days in each case. The dotted line is a least square fit to the quasi-regular and irregular bursts and is shown here for comparison. For both the types of regular bursts, the burst duration is constant for each day but it does show day to day variation. It may be stressed here that although the regular bursts themselves do not show any correlation between the preceding quiescent time and the burst duration, they fall very close to the relation derived for the quasi-regular and irregular bursts (see inset of Figure 5). We do not find any correlation between the quiescent time following the burst and the burst duration and results for 257 different type of bursts are shown in Figure 7. The observed correlation for the burst dura-

tion and the preceding quiescent time for the irregular and quasi-regular bursts could be simply a reflection of the fact that the burst duration and the quiescent time are of comparable magnitude for such bursts. This correlation, however, establishes that a given burst cycle starts at the beginning of a quiescent phase and gets completed at the end of a burst phase because we do not find any correlation between the burst duration and the following quiescent time. Henceforth, we shall use the preceding quiescent time as the quiescent time of a burst. It is interesting to note that we have observed continuously the full cycle of regular - irregular - quasi-regular and again regular bursts from June 17 to June 22, 1997.

We have calculated the average flux during the burst phase and during the quiescent phase separately for all the different type of observed bursts and results are shown in Figure 8. The ratio of average flux during the burst time to the average flux during the quiescent phase is plotted as a function of the burst duration. For quasi-regular and irregular bursts, this ratio shows good correlation with the burst duration (least square fit straight line) and has a value of two and higher. This ratio is, however, constant and has a value of less than two for the regular bursts as shown in the inset of Figure 8. The dotted line shows the least square straight line fit for the quasi-regular and irregular bursts.

We have calculated average hardness ratio during the quiescent phase for all types of bursts and results are shown in Figure 9. The hardness ratio decreases as the quiescent time increases and it is higher for the regular bursts than that for the quasi-regular and irregular bursts. The ratio of average flux during the burst time to the average flux during the quiescent phase is plotted in Figure 10 as a function of the average hardness ratio during the quiescent phase for all the observed bursts. The solid line is a least square fit to both types of regular burst data (442 regular bursts) which shows good correlation.

#### 5. DISCUSSION

Because of their unique feature of slow rise and fast decay, the bursts in GRS 1915+105 are very different from the type I X-ray bursts seen in about 40 LMXBs and type II X-ray bursts in the Rapid Burster (MXB 1730–335). All the bursts in the LMXBs have fast rise time of less than a second to a few seconds and slow decay of 10 sec-

onds to a few minutes (Lewin et al. 1995). The type I X-ray bursts are understood to be thermonuclear flashes caused by accretion of matter on to the surface of the neutron star. The type II bursts are produced by sudden infall of matter on to the neutron star due to some instability in the inner part of the accretion disk supported by the magnetic field. The slow decay of the burst intensity represents the cooling time scale of the neutron star photosphere. In the classical bursts, the spectrum is initially hard and becomes softer as the burst decays (Lewin et al. 1995). In sharp contrast, the bursts in GRS 1915+105 remain hard till the end and it is, in fact, the hardest near the end of the burst.

In the case of type I X-ray bursts, the ratio of the burst luminosity ( $L_b$ ) and the average quiescent X-ray luminosity ( $L_p$ ) is  $\frac{L_b}{L_p} \sim 10^{-2}$ . On the other hand, the time-averaged type II burst luminosity is much higher, usually 0.4 to 2.2 times the average luminosity of quiescent emission (Lewin et al. 1995). The time-averaged luminosity of the regular bursts detected from GRS 1915+105 is from 0.15 to 0.9 times the luminosity of the quiescent emission. This is much higher than the ratio in type I bursts (where the thermonuclear process has much smaller efficiency compared to the gravitational process) and less than the type II bursts (where the burst emission is due to gravitational energy release). The emission process involved in producing the bursts here is not likely to be thermo-nuclear because of the energetics involved. If the energy generation process is gravitational (like in type II bursts), the difference in efficiency might indicate the absence of hard surface in the compact object. A process in which the energy produced is due to gravitational potential but not all the energy is emitted as radiation, part of it being advected into the event horizon as kinetic energy of the matter, is appropriate for this source. This probably provides a compelling evidence that the compact object in GRS 1915+105 may be a black hole.

The quasi-regular and irregular bursts show higher variability near the end of the burst as we noted earlier and the burst duration is correlated to the quiescent time. Similar behavior is also reported from the PCA observations carried out in 1996 June (Belloni et al. 1997a). Several irregular bursts, concurrent with the present observations on 1997 June 18 and having similar properties,

have also been detected in the PCA data (Belloni et al. 1997b). They modeled these bursts as a consequence of emptying and replenishing of the inner accretion disk caused by a viscous thermal instability. Paul et al. (1998b), on the other hand, attempted to explain the regular bursts as due to periodic in-fall of matter onto a black hole from an oscillating shock front. In the following we attempt to give a comprehensive picture of the various types of bursts observed in GRS 1915+105 in the light of the recent theories of advective accretion disks.

### 5.1. *Advective accretion flows around black holes*

Recent work on the theory of accretion onto black-holes (see Abramowicz and Percival 1997; Chakrabarti 1996b; Narayan et al. 1998 for reviews) has shown that advection cooling is important in the innermost part of the accretion disk. For hot optically thin disks strong advective cooling occurs everywhere, very far from the black hole as well. Narayan & Yi (1994) have taken a self-similar solution and have divided the possible solutions into two branches: the first type where the energy is trapped from the disk and converted to jets and the second type with advection dominated thick accretion disk. A few observed sources are compared with the predictions of the Advective Dominated Accretion Flows (ADAF) with a fair degree of success (Narayan et al. 1997b). Chakrabarti & Titarchuk (1995), on the other hand, have taken a complete solution of viscous transonic equations and demonstrated that the accretion disk has a highly viscous Keplerian part which resides on the equatorial plane and a sub-Keplerian component which resides above and below it. The sub-Keplerian component can form a standing shock wave (or, more generally, a centrifugal barrier supported dense region) which heats up the disk to a high temperature. The need to define the viscosity parameter is circumvented by taking two accretion rates: the accretion through the classical “standard” disk and the accretion through the sub-Keplerian component. Ebisawa et al. (1996) have attempted to explain the observed X-ray spectrum, particularly the change of spectral states in the black hole candidates, using this model. In both the models the change of spectral states are ascribed to the change over from a purely thin accretion disk (with advection occurring very close to the black hole) in the high-soft state to the advective disk

extending over a large distance in the low-hard state. The hard X-ray power-law component is ascribed to the Comptonisation spectrum from the advective disk and the Shakura-Sunyaev multi-temperature disk emission (which is predominant in energies below  $\sim 10$  keV) is associated with the standard thin disk. In the ADAF model of Narayan & Yi (1994) the advective thick disk changes into a standard thin disk at a distance  $r_{tr}$  whereas according to Chakrabarti & Titarchuk (1995) the advective thick disk and the standard thin disk co-exist upto a certain radial distance and a standing shock wave or a centrifugal barrier dominated dense region is a common feature of the sub-Keplerian component. In the following we try to examine the burst properties of GRS 1915+105 in the light of these new accretion disk theories incorporating advection.

The source was in a low-hard state during 1996 December to 1997 March (Greiner et al. 1998) when the hard X-ray spectral index ( $\sim 2.0$ ) and the soft X-ray flux (300 - 500 mCrab) were low. The source started a new outburst around 1997 April-May when the soft X-ray flux started increasing and the X-ray spectrum became soft (spectral index increased to 3 - 4). We suggest that the peculiar bursts that we have seen are characteristics of the change of state of the source.

In the quiescent state of the burst the source is in the hard state. This is evident from the large value derived for the inner disk radius ( $R_{in}$ ) of the multi-temperature thin-disk model fitted for the energy spectrum. The fitted value of  $R_{in}$  is around 300 km for very long bursts of 1000 s duration (Belloni et al. 1997a) and 30 - 100 km for the irregular bursts (Belloni et al. 1997b) and 30 km for regular bursts (Taam et al. 1997). Note that the derived values for the radius can be underestimate due to scattering effects and also due to the approximation involved in fitting the Comptonised part of the spectrum as a power-law (see Shrader & Titarchuk 1998). It should be further noted here that the derivation of  $R_{in}$  is very much model dependent and we use this quantity only for a qualitative description of the spectral states and also to make an order of magnitude estimate of time scales involved in the change of spectral states. The fitted temperature of the disk is 1 - 1.5 keV. The spectral index of the power-law component during the quiescent state of the long bursts is  $\sim 2.22$  (Belloni et al. 1997a) indicating that the source is truly in a hard state. During

the burst phase the intensity is higher, the radius of the disk is smaller (20 - 30 km), the temperature is higher (2 - 3 keV) and the power-law index is steeper (3.57 for the long bursts and 3.3 for the regular bursts). These characteristics strongly suggest that the source is in a high-soft state during the bursts. Hence there are strong indications that the source makes state transitions in very short time scales corresponding to the rise and fall time of the bursts (a few seconds). Such fast changes of states are possible in the two component accretion flows where the advective disk covers the standard thin disk (Chakrabarti 1996b). In the following we describe the bursting behaviors of GRS 1915+105 within this scenario, taking the model parameters given in Chakrabarti & Titarchuk (1995) and also in Narayan et al. (1998).

In the low-hard state of the source the thin Keplerian disk is visible only from a large radial distance  $R_o$ , the sub-Keplerian component completely encompasses the thin disk below this radius (the soft photons from the disk act as seeds for the Comptonisation process). When the disk accretion rate ( $\dot{m}_d$ ) increases, at some critical point, the non-Keplerian halo accretion rate ( $\dot{m}_h$ ) can decrease and the high-soft state can set in. This change in accretion rate can occur either due to the change in the total accretion rate ( $\dot{m}_t = \dot{m}_d + \dot{m}_h$ ) or due to some changes in the viscosity in the thin accretion disk which changes  $\dot{m}_d$  (keeping  $\dot{m}_t$  constant). We suggest that when the total accretion rate is close to some critical value the source can change states and the observed irregular bursts are the manifestations of such changes of state.

To understand the mechanism of the bursts let us equate  $R_{in}$  to  $R_o$  from where the advection dominated halo component starts covering the thin accretion disk in the low-hard state of the source (the quiescent state of the burst). Assume that  $\dot{m}_d$  is close to a critical value where the change of the state takes place. At some particular point of time the boundary condition at the inner edge changes such that  $\dot{m}_d$  increases. The spectral state, however, will remain unchanged till this effect reaches  $R_o$ . The time scale for this to happen is the viscous time scale of the thin accretion disk. Assuming the standard  $\alpha$  disc we can write the viscous time scale as  $R_o^2/\nu$  where  $\nu$  is the viscosity coefficient which is given as  $\alpha c_s H$  for the  $\alpha$  disk, where  $c_s$  is the sound speed and  $H$  is the



disk thickness, and  $\alpha$  is the viscosity parameter. Taking the scaling laws for  $H$  and  $c_s$  (Frank, King & Raine 1985), we can write the viscous time scale of the disk as

$$t_{vis}^d = 4.3 \times 10^{-4} \alpha^{-1} \dot{m}_d^{-1} m^{-1} R_o^2 \text{ s} \quad (1)$$

where  $\dot{m}_d$  is in the units of Eddington accretion rate and  $m$  is the mass of the black hole in solar mass units and  $R_o$  is in km. Substituting  $\dot{m}_d = 1$ ,  $m = 10$ ,  $\alpha = 0.01$ , and  $R_o = 300$ , we get  $t_{vis} = 400$  s, agreeing with the observed quiescent state time scale of long bursts. This also explains the non-linear dependence of burst quiescent time with radius reported by Belloni et al. (1997b) for the long irregular bursts.

At  $R_o$ , the increased  $\dot{m}_d$  decreases  $\dot{m}_h$  and the advection dominated halo component completely advects onto the black hole in the viscous time scale of the halo component given by

$$t_{vis}^h = \frac{R_o^2}{H \alpha c_s} \quad (2)$$

Here we assume that the halo component is an advection dominated accretion disk in which the temperature can go very high (see Narayan et al. 1998). For advection dominated thick disks we can take  $H \sim R$  and use the scaling law for  $c_s$  as

$$c_s = 1.18 \times 10^{10} (R_o/R_s)^{-\frac{1}{2}} \text{ cm s}^{-1} \quad (3)$$

where  $R_s$  is the Schwarzschild radius (Narayan et al. 1998). We can rewrite the viscous time scale as

$$t_{vis}^h = 4.9 \times 10^{-6} \alpha^{-1} m^{-\frac{1}{2}} R_o^{\frac{3}{2}} \text{ s} \quad (4)$$

Substituting the values as earlier, we get  $t_{vis}^h$  as  $\sim 1$  s, which is quite close to the observed rise time of the burst. Now the burst phase starts, which is nothing but the soft state of the source with  $R_o$  coming very close to the shock front (or the centrifugal barrier supported dense region). Note that the value of  $R_o$  derived by spectral fitting is always 20 - 30 km during the burst maximum, irrespective of the type of the burst. At some particular time the inner boundary condition can change again and  $\dot{m}_d$  can decrease and  $\dot{m}_h$  can increase and this sub-Keplerian component can suppress inner part of the accretion disk and a Compton cloud can be generated. In the advection dominated accretion flow the radial velocity, typically, will be

$$v = -1.9 \times 10^{10} \alpha R_o^{-\frac{1}{2}} m^{\frac{1}{2}} \text{ cm s}^{-1} \quad (5)$$

(see Narayan et al. 1998). For a radius of 300 km, this will have a time scale of  $\sim 1$  s, which is seen as the fast decay time of the bursts.

For smaller values of  $R_o$ , the in-fall time scale will be lower (it goes as  $R_o^{\frac{3}{2}}$ ) and for some particular value of  $R_o$  this time scale can match the cooling time scale of the post shock region, which is about 0.01 s for a shock radius  $20 r_g$  (where  $r_g$  is the Schwarzschild radius) and black hole mass of  $10 M_\odot$  (Paul et al. 1998b). When the two time scales match they can give rise to oscillations which are quasi-periodic in nature (Molteni et al. 1996). The in-falling matter can immediately trigger the instability at the inner boundary of the disk and the source can immediately revert back to the hard state. These regular oscillations accumulate matter at the shock-front (or the centrifugal barrier) and they can catastrophically fall onto the black-hole. The scenario described above explains in a qualitative way the various types of bursts observed in GRS 1915+105. We must mention here that the time scales and sizes that we have taken for the calculations are very approximate due to the uncertainties in the multi-temperature disk parameters and the viscosity parameter.

The scenario sketched above is similar to that described by Belloni et al. (1997a) as far as the viscous time scale is concerned. These authors, however, make the assumption that when the source reverts back to the low intensity state of the burst, the matter between  $R_o$  and  $R_i$  disappears behind the black hole at a free fall time scale. It is worth pointing out that a standard thin accretion disk cannot disappear at free-fall time scale without effectively transferring its angular momentum and the time scale for angular momentum transfer is the viscous time scale. Further, the systematic change in the hard power-law index during the bursts cannot be explained by only invoking a change in the disk inner radius.

Paul et al. (1998b) have explained the regular bursts in terms of the oscillations of the shock front. For this to happen in the observed time scale, the shock has to be very far away from the black hole. This can only happen in the low state of the source. Actual observations, however, suggest that the regular bursts occur when the source approaches the soft-high state when

the shock front is very close to the compact object. Hence it appears that the periodicity of the regular bursts occurs from the matching of the viscous time scales rather than the shock front oscillation. The catastrophic in-fall of matter at the shock-front, invoked by Paul et al. (1998b), seems to be appropriate for the regular bursts.

Several of the correlations obtained in the preceding sections can be explained using the physical picture described above. The quiescent flux is related to  $R_o$  (see Table 2). The rise time of the bursts represents the viscous time scales of the halo component. The burst duration is related to the preceding quiescent time (Figure 5) because the time scale for the inner boundary condition to change will also be the viscous time scale, which is related to the  $R_o$  of the preceding quiescent time. This correlation does not hold for the regular bursts because the burst duration is independent of  $R_o$  due to the resonance. During quasi-regular and irregular bursts, change in  $\dot{m}_d$  is mainly due to change in viscosity caused by a viscous - thermal - instability (see Figure 9; the variation in hardness ratio for these bursts during quiescent time is much less than that in case of regular bursts) (Belloni et al. 1997a). The high quiescent time X-ray flux during the regular bursts heats up the disk and suppresses the instability (Lewin et al. 1995).

The ratio of the average fluxes during the burst and the quiescent time essentially represents the ratio of the values for  $R_o$  which is related to the burst duration through the relation for the viscous time scale (Figure 8). The hardness ratio (which represents the inner disk temperature) shows weak dependence on the quiescent time for the irregular bursts because for large enough  $R_o$  the temperature does not change drastically with  $R_o$  (Figure 9). The regular bursts of long duration (45 s) also have a value for the hardness ratio during quiescent time which is similar to that seen for the irregular bursts (though slightly higher). The variation in hardness ratio is larger which reflects the change in  $R_o$  (see Figure 10). The mean burst hardness ratio for these bursts is  $\sim 1.2$  which suggests that these bursts occur during high state (Narayan et al. 1998). During the short duration regular bursts the source is almost in the soft-high state during the quiescent phase, showing a large value for the hardness ratio. The mean burst hardness ratio is  $\sim 2.2$  which suggests very high state. These observations imply that

$\dot{m}_d$  is substantially larger in very high state than that in high state. The flux ratio for the regular bursts represents the amount of amplification that is possible for the resonating bursts and it is related to the quiescent time temperature (Figure 10).

According to the scenario sketched above, the X-ray bursts are due to fast changes in the spectral states when the source reaches the high state and the accretion rate is very close to the Eddington accretion rate. Chakrabarti & Titarchuk (1995) have pointed out that during such high state the source shows distinct hard spectral component due to bulk motion Comptonisation. Shrader & Titarchuk have fitted the high state spectrum of GRS 1915+105 using the bulk motion Comptonisation model and derived a temperature of 0.9 keV. Titarchuk & Zannias (1998) have analyzed the exact general relativistic integro-differential equation of radiative transfer for a realistic situation of accretion onto black holes in the high state and showed that an extended power-law spectrum results even from an arbitrary spectrum of low energy photons. Laurent & Titarchuk (1998) have calculated the specific features of X-ray spectra using Monte-Carlo simulations and demonstrated the stability of power law spectral index over a wide range of mass accretion rate. This conclusion agrees with our observation that the hardness ratio during the quiescent time remains constant over wide burst time scales (Figure 9), except for the regular bursts of 21 s duration which may be due to reduced optical depth (thus the halo) for these bursts.

It is interesting to speculate the possible reasons for the differences in the two regular bursts of  $\sim 21$  s and  $\sim 46$  s duration. As pointed out by Shrader & Titarchuk (1998), bulk motion Comptonisation sets in during the soft-high state and the energy radiated is a very small fraction of the accretion energy. Part of the energy can be used to drive the matter away from the central source in terms of jets. The difference in the two regular bursts may be due to the fact that in the regular bursts of 21 s duration jet formation may be setting in. It may be noted here that the time profiles of the two types of regular bursts agree with each other but for a sharp dip in the short regular bursts.

The ADAF models have been used to obtain unique identifying features of black hole sources (Narayan et al. 1997a; Laurent & Titarchuk

1998). An advection-dominated accretion flow is one in which most of the energy released by viscous dissipation is stored in the gas and advected to the compact object and a small fraction of the energy is radiated. The argument is that if accretion is via an ADAF and if the object has an event horizon, then the advection energy will disappear from sight. However, if the central object has a surface, then the surface will be heated by the hot inflow from the ADAF and the advected energy will be emitted as thermal radiation. This additional evidence for the black hole nature of GRS 1915+105 is qualitatively different from usual method that rely on a measurement of the mass. The usual argument is that if an object is too massive to be a neutron star it must be a black hole.

### 5.2. A test of the model using RXTE/PCA data

In principle, one can test this model using X-ray data above 10 keV. The Shakura-Sunyaev multi-temperature disk emission dominates in 2–10 keV energy range while the power-law component dominates at higher energies (Shrader & Titarchuk 1998). We have analysed the publicly available RXTE/PCA data for irregular as well as regular bursts concurrent with our observations. The results of irregular bursts from RXTE/PCA data of 1997 June 18 are shown in Figure 11 along with the results from RXTE/PCA data of 1997 May 8 and August 19 when GRS 1915+105 was in low state and in high state respectively. Both the top panels and the bottom panels have same Y-axis scales. Similarly, both the left panels and the right panels (top and bottom) have same X-axis scales. This allows straight forward comparison of burst time data with the data during low and high state. GRS 1915+105 was in high state on 1997 August 19 and 2–13 keV flux varied from 19000 c/s to 30000 c/s while the source was in low state on 1997 May 8 and 2–13 keV flux was steady around 6000 c/s (right top panel). No burst is observed during these observations. The ratio of 13–60 keV flux to 2–13 keV flux has a value of  $12 \pm 2$  % during the low state on 1997 May 8 while it is  $\sim 3$  % during the high state on 1997 August 19 (bottom right panel). This implies that the source remains in the same state during these observations.

The results of irregular bursts on 1997 June 18 are shown in left panels of Figure 11. The 2–13 keV flux varies from 4000 c/s to 28000 c/s which is

shown in left top panel. These bursts have similar profile as those shown in second panel (from top) of Figure 1 from our data of 2–18 keV for June 27. The ratio of 13–60 keV flux to 2–13 keV flux is shown in left bottom panel. The relative flux of 13–60 keV reaches upto 12% during quiescent time while it is as low as only 3% during burst phase of irregular bursts. The minimum value of this ratio during burst phase is in agreement with the value of this ratio for high state on 1997 August 19. Similarly, its maximum value during quiescent phase is in agreement with the value for low state on 1997 May 8. The 13–60/2–13 ratio drops to its minimum value of  $\sim 3$  % at the first peak of each burst which implies the cooling of the halo component by the soft photons from the disk. It starts increasing immediately during the rest of the burst phase. This ratio reaches a value of  $\sim 6$  % during the burst decay phase which would mean a significant recovery of the halo component. The burst decay phase, therefore, may represent unsaturated Comptonisation before the source reaches saturated level of low state.

Similar results of regular bursts from RXTE/PCA data of 1997 June 22 are shown in Figure 12. The 2–13 keV flux varies from 7000 c/s to 29000 c/s (top panel). The ratio of 13–60 keV flux to 2–13 keV flux reaches upto 9% during quiescent time and it drops upto  $\sim 3.5$  % during burst phase of regular bursts (bottom panel). One would expect higher contribution from power-law component due to larger  $R_0$  in case of irregular bursts than that for regular bursts. It would mean that resonance terminates the recovery of the halo component prematurely in the case of regular bursts. In fact, it is the major difference between the regular bursts and the irregular bursts as much longer time is available for the recovery of the halo component in the case of irregular bursts. During bursts phase, the relative contribution of power-law component is lower in case of regular bursts as thin accretion disk extend to smaller radius and hence has higher temperature than that for irregular bursts (see Figure 10). The results of the other type of regular bursts of  $\sim 21$  s duration are also consistent with this scenario. The ratio of 13–60 keV flux to 2–13 keV flux reaches upto 6% during quiescent time. The 2–13 keV maximum flux during burst phase is same (approaching a value of 28000 c/s for 5 CPUs of RXTE/PCA) for all the types

of observed bursts, provides another independent support to our model while the quiescent time minimum flux varies almost by a factor of four.

## 6. CONCLUSION

The observed bursts from GRS 1915+105 are very different compared to the classical bursts in the LMXBs both in terms of temporal structure and spectral evolution. Our results broadly put all the observed bursts in two classes: irregular and quasi-regular bursts in one class, and regular bursts in another class. There is strong correlation between the preceding quiescent time and the burst duration for the quasi-regular and irregular bursts. No such correlation is found for the regular bursts. The ratio of average flux during the burst time to the average flux during the quiescent phase is high and variable in former case while it is low and constant in latter case. We present a comprehensive picture of the various types of bursts observed in GRS 1915+105 in the light of the recent theories of advective accretion disks. We present a unified model for the origin of these bursts which explains almost all the observed properties of these bursts. We suggest that the peculiar bursts that we have seen are characteristic of the change of state of the source. The

change of state is due to change in the disk accretion rate which may be either due to a change in the total accretion rate or due to some changes in the viscosity in the thin accretion disk. The periodicity of the regular bursts occurs from matching of the viscous time scale with the cooling time scale of the post shock region. We have presented a test of this model using 13–60 keV RXTE/PCA data for irregular bursts and regular bursts, during the low-hard state, and during the high-soft state which show good agreement with our model. These results may be viewed as additional evidence that the X-ray source GRS 1915+105 is a black hole.

We thank K. P. Singh for the valuable comments on the manuscript. We acknowledge K. Thyagrajan, Project Director of IRS-P3, R. N. Tyagi, Manager PMO and staff of ISTRAC for their support during observations. The valuable contributions of the technical and engineering staff of ISAC and TIFR in making the IXAE payload are gratefully acknowledged. We thank RXTE team for making their data publicly available. We are grateful to the anonymous referee for his constructive comments and suggesting improvements.

## REFERENCES

- Abramowicz, M. A., & Percival, M. J. 1997, *Class. Quantum Gravity*, 14, 2003  
 Agrawal, P. C., et al. 1996, *IAU Circ.* 6488  
 Agrawal, P. C., et al. 1997, *Journal of the Korean Astronomical Society*, 29, S429  
 Belloni, T., et al. 1997a, *ApJ*, 479, L145  
 Belloni, T., et al. 1997b, *ApJ*, 488, L109  
 Bradt, H. 1996, preprint.  
 Castro-Tirado, A. J., et al. 1994, *ApJS*, 92, 469  
 Chakrabarti, S. K., & Titarchuk, L. G. 1995 *ApJ*, 455, 623  
 Chakrabarti, S. K. 1996a, *ApJ*, 464, 664  
 Chakrabarti, S. K. 1996b, *Phys. Rep.*, 266, 229  
 Eikenberry, S. S., et al. 1998, *ApJ*, 494, L61  
 Ebisawa, K., Titarchuk, L., & Chakrabarti, S.K. 1996, *PASJ*, 48, 1  
 Frank, J., King, A. R., & Raine, D. J. 1985, *Accretion Power in Astrophysics*, Cambridge: Cambridge University Press, p. 86  
 Greiner, J., Morgan, E. H., & Remillard, R. A. 1996, *ApJ*, 473, L107  
 Greiner, J., Morgan, E. H., & Remillard, R. A. 1998, *astro-ph/9806323*  
 Laurent, P., & Titarchuk, L. 1998, *astro-ph/9808015*  
 Lewin, W. H. G., Jan Van Paradijs, & Taam, R. E. 1995, in *X-ray Binaries*, eds. Lewin., W. H. G., Jan Van Paradijs, & van den Heuvel, Cambridge: Cambridge University Press, p. 175-232  
 Mirabel, I. F., & Rodriguez, L. F. 1994, *Nature*, 371, 46  
 Mirabel, I. F., et al. 1998, *A & A*, 330, L9  
 Molteni, D., Sponholz, H., & Chakrabarti, S. K. 1996, *ApJ*, 457, 805  
 Narayan, R., & Yi, I. 1994, *ApJ*, 428, L13  
 Narayan, R., Garcia, M. R., & McClintock, J. E. 1997a, *ApJ*, 478, L79  
 Narayan, R., Barret, D., & McClintock, J.E. 1997b, *ApJ*, 482, 448  
 Narayan, R., Mahadevan, R., & Quataert, E. 1998, To appear in *The Theory of Black Hole Accretion Disks*, Eds: M.A. Abramowicz, G. Bjornsson, & J.E. Pringle (Cambridge University Press); *astro-ph/9803141*  
 Orosz, J. A., & Bailyn, C. D. 1997, *ApJ*, 477, 876  
 Paul, B., et al. 1997, *A & A*, 320, L37  
 Paul, B., et al. 1998a, *A & A Suppl. Ser.* 128, 145  
 Paul, B., et al. 1998b, *ApJ* 492, L63  
 Rao, A. R., et al. 1998, *A & A*, 330, 181  
 Shrader, C., & Titarchuk, L. 1998, *ApJ*, 499, L31  
 Taam, R. E., Chen, X., & Swank, J. H. 1997, *ApJ*, 485, L83  
 Tanaka, Y., & Lewin, W. H. G. 1995, in *X-ray Binaries*, eds. Lewin., W. H. G., Jan Van Paradijs, & van den Heuvel, Cambridge: Cambridge University Press, p. 166  
 Titarchuk, L., & Zannias, T. 1998, *ApJ*, 493, 863

## FIGURE CAPTIONS

FIG. 1.— The regular bursts with  $\sim 21$  s recurrence time (first panel from the top), irregular bursts (second panel), quasi-regular bursts (third panel) and regular bursts with  $\sim 46$  s recurrence time (fourth panel) observed in GRS 1915+105 with all the PPCs except on June 27 (irregular bursts) when only PPCs 2 & 3 were on. Date of each observation is given in the respective panels. The regular bursts observed by RXTE/PCA on June 22 are shown in bottom panel for comparison with the regular bursts observed on June 22 with the PPCs. For other details see in text.

FIG. 2.— The mean burst recurrence time for each day of observation. The error bars show  $1\sigma$  variation in each day of observation.

FIG. 3.— (a) The burst profiles in two different energy bands are shown in the top panels for the two types of regular bursts. The hardness ratio is shown in the bottom panels and (b) the burst profiles in two different energy bands are shown in the top panels for the quasi-regular and irregular bursts. The hardness ratio is shown in the bottom panels.

FIG. 4.— The rise and decay segments of the burst profile of all four types of observed bursts. The start time of the bursts is arbitrarily chosen at 0 s and the end time at 40 s for clarity of comparison. The intensity of the rising segment is normalized to the start point while intensity of the decay segment is normalized to the end point.

FIG. 5.— Correlation between the preceding quiescent time and the burst duration (as defined in the text) for the quasi-regular and irregular bursts. The straight line is the least square fit to the data. In the inset, both types of regular bursts are also shown.

FIG. 6.— Correlation between the preceding quiescent time and the burst duration for the regular bursts with  $\sim 21$  s recurrence time in the top panel and for the regular bursts with  $\sim 46$  s recurrence time in the bottom panel. Data are for three days in each case. The least square fit for the quasi-regular and irregular bursts (of Figure 5) is shown by dotted line for comparison.

FIG. 7.— Correlation between following quiescent time and the burst duration (as defined in the text) for the same data as in Figure 5.

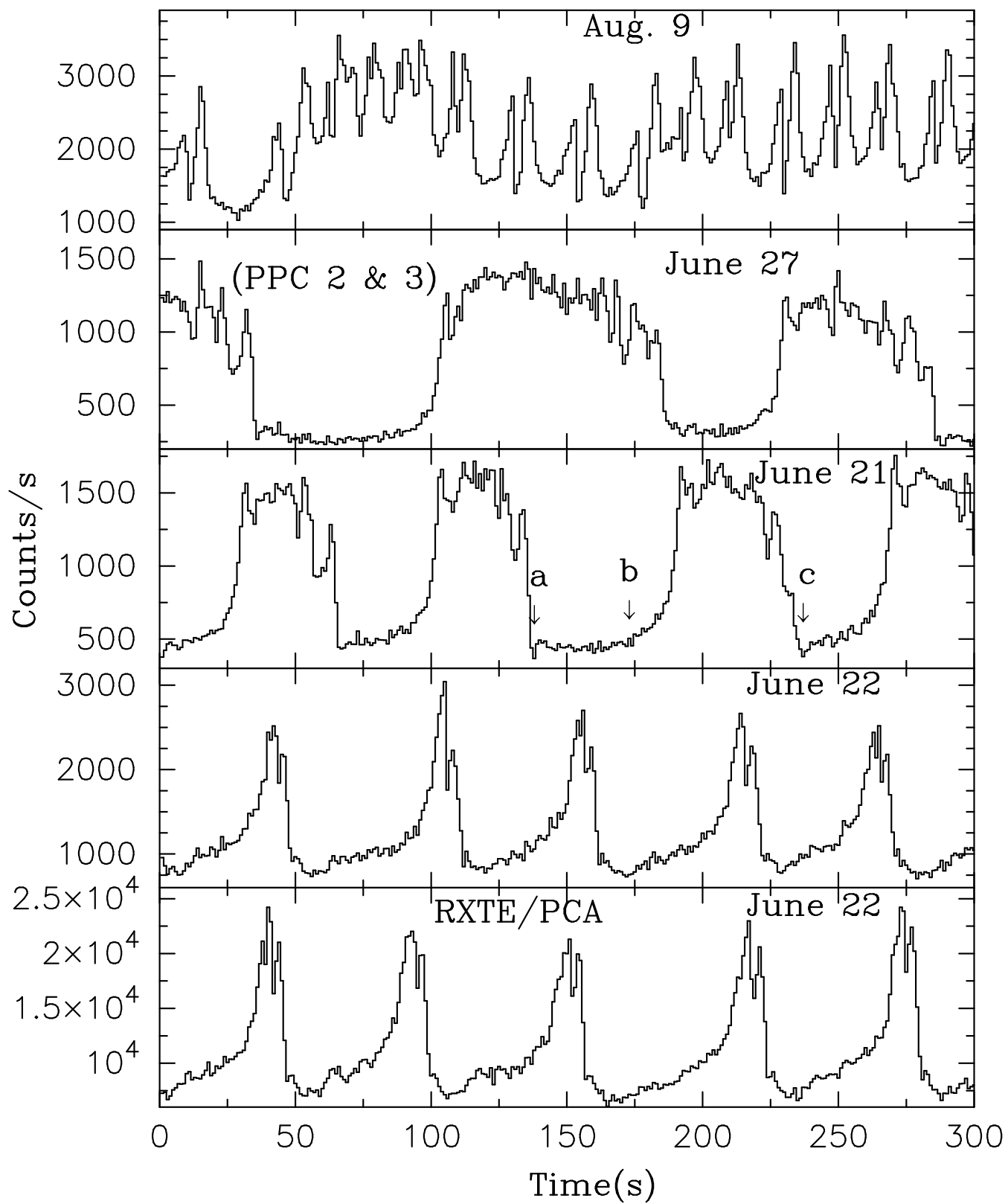
FIG. 8.— The ratio of the average flux during burst to the average flux during quiescent time as a function of the burst duration for the quasi-regular and irregular bursts. The solid line is the least square fit to the data. In the inset, results for both the type of regular bursts are shown. The dotted line is the fit for the quasi-regular and irregular bursts shown for comparison.

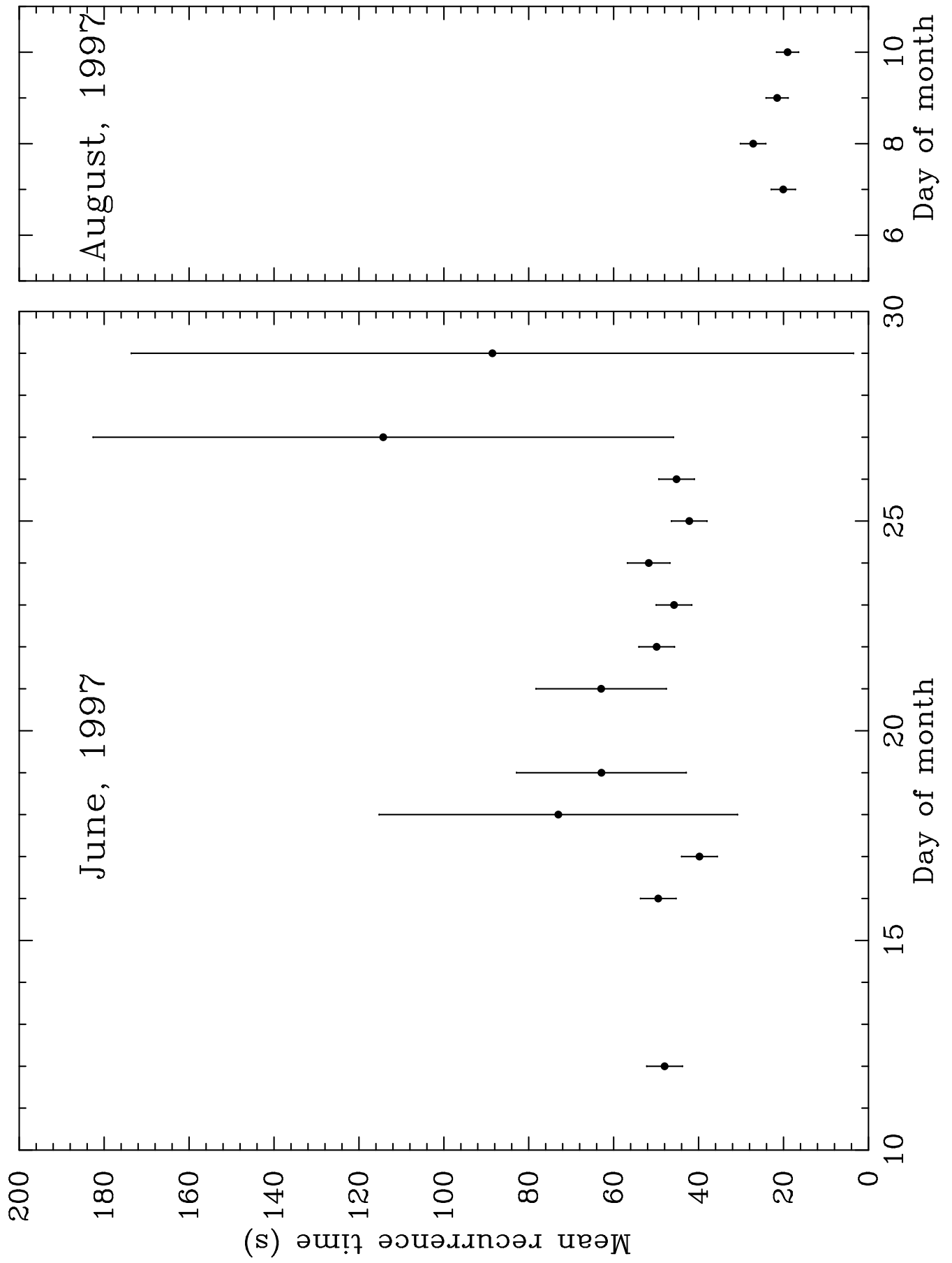
FIG. 9.— The hardness ratio during the quiescent phase vs the quiescent time for all the type of observed bursts from GRS 1915+105.

FIG. 10.— The ratio of the average flux during burst to the average flux during the quiescent time as a function of the hardness ratio during the quiescent time for all the type of observed bursts. The least square fit to both the type of regular bursts is shown by a solid line.

FIG. 11.— Plot of 2–13 keV flux vs time is shown in left top panel (irregular bursts) and the ratio of 13–60 keV flux to 2–13 keV flux is plotted as a function of time in the left bottom panel from RXTE/PCA data of 1997 June 18. In the right top panel, 2–13 keV flux is plotted from RXTE/PCA data of 1997 August 19 and May 8 when source was in high and low states respectively. Respective ratios of 13–60 keV flux to 2–13 keV flux are plotted in the right bottom panel.

FIG. 12.— Plot of 2–13 keV flux vs time is shown in the top panel (regular bursts) and the ratio of 13–60 keV flux to 2–13 keV flux is plotted as a function of time in the bottom panel from RXTE/PCA data of 1997 June 22.





## Different types of X-ray bursts

